Biosensors and Bioelectronics 89 (2017) 1059–1067

Contents lists available at ScienceDirect

Biosensors and Bioelectronics

journal homepage: www.elsevier.com/locate/bios

A highly sensitive and specific capacitive aptasensor for rapid and label-free trace analysis of Bisphenol A (BPA) in canned foods

Hadi Mirzajani[a,b], Cheng Cheng[a], Jayne Wu[a,*], Jiangang Chen[c], Shigotoshi Eda[d], Esmaeil Najafi Aghdam[b], Habib Badri Ghavifekr[b]

[a] The University of Tennessee, Knoxville, Department of Electrical Engineering and Computer Science, 1520 Middle Drive, Knoxville, TN 37966, USA
[b] Sahand University of Technology, Department of Electrical Engineering, Microelectronics Research Lab., Tabriz, Iran
[c] The University of Tennessee, Department of Public Health, 1914 Andy Holt Avenue, Knoxville, TN 37996, USA
[d] University of Tennessee Institute of Agriculture, Department of Forestry, Wildlife and Fisheries, 2431 Joe Johnson Drive, Knoxville, TN 37996, USA

ARTICLE INFO

Keywords:
Capacitive biosensor
AC electrokinetics (ACEK)
Point-of-care (POC) diagnostics
Small molecule detection

ABSTRACT

A rapid, highly sensitive, specific and low-cost capacitive affinity biosensor is presented here for label-free and single step detection of Bisphenol A (BPA). The sensor design allows rapid prototyping at low-cost using printed circuit board material by benchtop equipment. High sensitivity detection is achieved through the use of a BPA-specific aptamer as probe molecule and large electrodes to enhance AC-electroelectrothermal effect for long-range transport of BPA molecules toward electrode surface. Capacitive sensing technique is used to determine the bounded BPA level by measuring the sample/electrode interfacial capacitance of the sensor. The developed biosensor can detect BPA level in 20 s and exhibits a large linear range from 1 fM to 10 pM, with a limit of detection (LOD) of 152.93 aM. This biosensor was applied to test BPA in canned food samples and could successfully recover the levels of spiked BPA. This sensor technology is demonstrated to be highly promising and reliable for rapid, sensitive and on-site monitoring of BPA in food samples.

1. Introduction

Bisphenol A (4,4′-(propane-2,2-diyl)diphenol, BPA) is known to be a compound extensively used in the production of polycarbonate and epoxy resin products. These materials are widely used in production of food and water containers including the inner surface coating of food cans (Crain et al., 2007; Yoshida et al., 2003). BPA has been shown to mimic the effect of endogenous hormones even at very low concentrations leading to adverse effects such as reproductive disorders, chronic diseases, and various types of cancer in vitro in animal model, although our understanding of the potential adverse health effects of BPA exposure in humans are still incomplete. (Huo et al., 2015; Mustieles et al., 2015; Oppeneer and Robien, 2015; Paseiro-Cerrato et al., 2016). U.S. Food and Drug Administration (FDA) estimated that BPA exposure from food contact materials is approximately 2.42 μg/kg bw/day and 0.185 μg/kg bw/day for infants and adults, respectively (FDA, 2014). Due to BPA's negative impact especially on children and infants, Canada and China banned the use of BPA in baby bottles in 2010 and 2011, respectively (Gao et al., 2012; Wu et al., 2012). In January 2011, the use of BPA in baby bottles was prohibited in all EU-countries. In January 2015, the European Food Safety Authority recommended the current Tolerable Daily Intake (TDI) level for BPA of 4 μg/kg body weight/day (Authority, 2015). In contrast, many other countries including Iran have not established a national standard on average daily intake and presence of BPA in food contact materials (Moghadam et al., 2012). BPA is still extensively used worldwide for production of food storage and packaging materials which makes public health highly vulnerable to its exposure and potential toxicity. Hence, there is an urgent need to develop sensitive and quantitative measurement methods for BPA detection specifically in various biological and aqueous food samples to facilitate risk assessment of human BPA exposure.

The conventional methods for low level BPA detection include high pressure liquid chromatography (HPLC) (Yoon et al., 2003), liquid chromatography (LC) (Shao et al., 2005), and liquid chromatography coupled with mass spectrometry (LC-MS) (Tominaga et al., 2006). These methods require multiple complicated sample processing steps, expensive equipment, and skilled personnel, which severely limits the accessibility of BPA detection methods. Thus, there is a huge need for the development of low cost, simple operation, and one-step-to-answer methods for quick on-site determination of BPA level directly from samples.

* Corresponding author.
E-mail address: jwu10@tennessee.edu (J. Wu).

http://dx.doi.org/10.1016/j.bios.2016.09.109
Received 20 July 2016; Received in revised form 24 September 2016; Accepted 30 September 2016
Available online 04 October 2016
0956-5663/

Table 1
Comparison of sensor characteristics between the sensor in this paper and previously reported methods.

Reference	Materials Detection method	Analytical range	LOD	Assay time	Selectivity test
(Zhu et al., 2015b)	Nanoporous gold film Electrochemical	0.1–100 nM	0.056 ± 0.004 nM	30 min	phenol, hydroquinone, 4,4′ –dihydroxybiphenyl and bisphenol B
(Cui et al., 2015)	Surface Acoustic Wave (SAW) Chips Capacitive	10 fM–10 pM	10 fM	20 s	Not conducted
(Pan et al., 2015)	Graphene-gold nano-composite Electrochemical	0.025–3 μM	1 nM	Not Mentioned	Not conducted
(Kim et al., 2015)	Recombinant protein-immobilized graphene electrodes Electrochemical	100 fM–10 nM	5 fM	30 min	BPS and BPF
(Singh et al., 2015)	Self assembled DC sputtered nanostructured rutile TiO_2 platform Impedimetric	0.01–1 μM	0.01 μM	250 s	HQ, PAP, PH, PNP, RS and their mixture
(Chung et al., 2015)	Double strand DNA-embedded Au/Ag core-shell nanoparticles Surface-enhanced Raman scattering	10 fM–100 nM	10 fM	40 min	6F, BP and BPB
(Reza et al., 2015)	Reduced graphene oxide sheets and chitosan polymer EIS[a]	0.01–50 μM	0.74 nM	10 s	Phenol, nitrophenol, 4 aminophenol, resorcinol and all mixers
(Zehani et al., 2015)	Diazonium-functionalized boron-doped diamond electrode modified with a multi-walled carbon nanotube-tyrosinase hybrid film Amperometric	0.01–100 nM	10 pM	Not Mentioned	2-nitrophenol, Ni^{+2}, Cd^{+2}, KNO3, Cu^{+2}, sucrose and glucose
(Zhu et al., 2015a)	Graphene Oxide FRET fluorescence signal	0.1–10 ng/mL	0.05 ng/mL	15 min	BPB, BPC, DEC, and BPE
(Wang et al., 2015)	Copper-centered metal-organic framework Electrochemical	0.05 μM – 3 μM	13 nM	11 s	common inorganic ions (such as 2 mM K^+, Na^+, $NO3^-$, $H_2PO_4^-$, $HPO4^{2-}$, Cl^- andAc^-) and organic solvents (such as 0.25% v/v acetone, acetonitrile, methanol and ethanol)
(Feng et al., 2016)	Gold heteroassemblies Surface-enhanced Raman scattering	0.001–1 ng/mL	3.9 pg/mL	Not Mentioned	BPC, DPA and DES
(Yu et al., 2016)	gold electrode EIS[a]	1 pM to 100 pM	0.19 pM	3 h	BPB, HBPA, and 6F-BPA
(Chen and Zhou, 2016)	DNA Y junction, exonuclease III-based signal protection strategy	10 fM – 10 nM	5 fM	90 min	BPE, BPB, BPC, BPF, 4BP, DES, E2, Estriol, and Atrazine
(Li et al., 2016a)	Disposable paper-based, stacked gold nanoparticles supported carbon nanotubes EIS[a]	0.2–20 mg/L	0.03 mg/L	Not Mentioned	Na^+, Mg^{2+}, K^+, Cl^-, $SO4^{2-}$, NO^{3-}, Cu^{2+}, Fe^{3+}, Zn^{2+}, Cr^{3+}, Ni^{2+}, catechol, HQ, PCP, p-NA and p-NP
(Kim et al., 2016)	Multichannel Carbon Nanofiber Transducer Sensor current I_{SD}	1 fM–10 pM	1 fM	150 s	4,4′-(butane-2,2-diyl) diphenol (Bisphenol B, BPB), 4,4-bis(4-hydroxyphenyl) valeric acid (VA), 4,4′-(hexafluoroisopropylidene) diphenol (6F), and 4,4′-dihydroxybiphenyl (4,4′- biphenol, BP)
(Guo et al., 2016)	Mn2+-doped NaYF4: Yb/Er upconversion nanoparticle Electrochemiluminescent	0.05–100 ng/mL	0.037 ng/mL	30 min	BPB, Phenol, HQ, Ca^{2+} and Mg^{2+}
(Li et al., 2016b)	CMK–3/nano-CILPE[b] EIS[a]	0.2–150 μM	0.05 μM	180 s	KCl, Na_2SO_4, $MgCl_2$, $CaCl_2$, $ZnCl_2$, $FeCl_3$, Na_2CO_3, $Cu(NO_3)_2$
(Wang et al., 2016)	Ionic liquid functionalized conducting polymer platform Cyclic voltammetry	0.1–500 μM	0.02 μM	Not Mentioned	$NaNO^3$, Na_2SO_4, Na_2CO_3, KCl, $CoCl_2$, $ZnCl_2$ and sodium citrate
This work	PCB-based Capacitive	1 fM–10 pM	152.93 aM	20 s	BPF and BPS

[a] Electrochemical Impedance Spectroscopy (EIS).
[b] Ordered mesoporous carbon CMK-3 modified nano-carbon ionic liquid paste electrode.

In recent years, several new sensing techniques based on different probe molecules such as enzymes (Kochana et al., 2015; Pan et al., 2015; Wang et al., 2014), aptamers (Cheng et al., 2016; Cui et al., 2015; 2016; Zhu et al., 2014, 2015b), antibodies (Wang et al., 2014), and peptides (Kim et al., 2015; Yang et al., 2014) have been developed and applied for high affinity and specificity BPA detection. Since BPA is a small molecule analyte, both aptamers and peptides are advantageous as probe molecule in affinity sensors. Additionally, they can be synthesized with high reproducibility and purity from commercial sources (Song et al., 2008), selected in vitro for any given target, and can be used for detection of small molecules up to large proteins and even viruses and parasites (Brogden, 2005; Hoyos-Nogués et al., 2016). Peptide probes provide better selectivity than aptamers. Due to charge neutrality of peptide, peptide probe can be immobilized at higher density than aptamer, often leading to larger dynamic range. However, currently, the availability and cost of peptide probe still limit its use. For this work, aptamer probe was used owing to its availability.

While aptasensors can work with several detection methods including optical, mass and electrochemical detection, sensors based on electrical sensing methods are cheaper and easier to implement than others, which is important for point-of-need applications. In the following, recent literature on using electrical aptasensors to detect BPA levels in food and drink samples is reviewed. Zhou et al. (2014) developed an electrochemical aptasensor for BPA detection in milk. The device was based on glassy carbon electrode (GCE) modified by gold nanoparticle-dotted graphene (GNPs/GR) nanocomposite film, which achieved a limit of detection (LOD) of 5 nM with detection time of 30 min. Yu et al. (2016) developed an electrochemical aptasensor based on triple-signaling strategy to detect trace level BPA in tap water. Their device had a linear range from 1 pM to 100 pM with an LOD of 0.19 pM. Guo *et al.* presented an aptasensor labeled with Mn^{2+}-doped $NaYF_4$:Yb/Er upconversion nanoparticles ($NaYF_4$:Yb, Er/ Mn UCNPs) that employed electrogenerated chemiluminescence (ECL) for detection of BPA in water (Guo et al., 2016). The device could detect BPA concentrations from 0.05 to 100 ng/mL with an LOD of 0.037 ng/mL. Xue et al. (2013) developed an electrochemical aptasensor capable of detecting BPA levels as low as 0.284 pg/mL in drinking water in less than 30 min. Kim et al. (2016) developed a field-effect transistor (FET) sensor using aptamer-modified multichannel carbon nanofibers (MCNFs) and achieved an LOD of 1 fM for BPA detection. Cheng et al. (2016) demonstrated an aptasensor fabricated by laser induced carbonization of flexible polyimide sheets for rapid detection of BPA in U.S. surface water. AC electroosmotic (ACEO) effect was integrated with capacitive sensing technique and the sensor could detect BPA at attomolar level in 20 s.

Many of the previously reported aptasensors have one or some of the following shortcomings: 1) They have relatively long turnaround time to provide the detection results, usually a few hours or even a day; 2) The reported LODs are still high, mostly in the range of nano/pico-molar, 3) Their linear dynamic range is limited. Most of them have 2 or 3 orders of magnitude; 4) More importantly, they require sophisticated and/or laborious process and equipment for fabrication and surface engineering of the sensor. These limitations potentially can restrict their acceptance for widespread diagnostic use.

Our previous work on small molecule detection has revealed that larger electrode will lead to improved detection sensitivity and limit of detection due to enhanced AC electrothermal flow (Cui et al., 2016). In addition, a large sensing area will lead to higher stability due to averaging effect. Furthermore, because the critical dimension of the sensor is increased, alternative low-cost fabrication techniques can be used for sensor fabrication. The BPA sensor presented in this paper is based on printed circuit board (PCB) technique. The materials used for fabrication are cheap and widely available. Moreover, it can be fabricated using compact, simple to operate and low cost benchtop equipment without sophisticated extensive surface engineering process for the sensor. The cost for each prototyped sensor is less than 50 cents. The preparation of the sensor involves only surface cleaning and biomolecular immobilization.

This reported method uses an optimized AC signal to interrogate the capacitance of the electrode sensors while inducing ACEK effects for accelerated transport of analyte toward the electrodes, where BPA-specific aptamer is immobilized. The BPA level is quantified by finding the interfacial capacitance change rate as a result of specific binding of BPA molecules with aptamer. The detection is label-free and single step. The sensor has a large linear range of 1 fM to 10 pM with an LOD of 152.93 aM and has a response time of 20 s.

In order to demonstrate the device performance, the operating characteristics of the ACEK capacitive sensor were compared with those of previously reported methods and summarized in Table 1. Overall, this sensor exhibits excellent performance in several aspects. The first is the low LOD of 152.93 aM, which is more sensitive than many BPA biosensors in the literature. Second, the sensor responds in seconds when exposed to BPA, whereas the turnaround time from other methods are in hours. In terms of the cost, the aptasensor utilizes PCB technique which is very cheap and facile to prototype through inexpensive materials and involve less intensive personnel training. Considering the above features, the PCB-based capacitive aptasensor has significant advantages for point-of-care applications.

2. Materials and methods

2.1. Sensing mechanism and sensor structure

2.1.1. Detection mechanism

The detection is based on interrogating the capacitance change at the interface between a sensor electrode and the sample solution due to binding reaction. For a bare electrode, its interfacial capacitor (C_{int}) arises from the electric double layer (EDL). When an electrode is immersed in the solution, the electrode surface will acquire surface charges. To maintain charge neutrality, counter ions are induced within a very thin layer at the electrode/liquid boundary to counter the surface charges at the electrode surface, which is commonly known as the EDL. By considering the layers of counter ions as one plate and the electrode surface as the other plate, the EDL can be electrically modeled as the interfacial capacitor (Mirzajani et al., 2016). When target molecules are collected over the electrode surface, the thickness of the interfacial capacitor will increase, which consequently decreases the interfacial capacitance of the IDE.

As schematically shown in Fig. 1(a), when the electrode is not functionalized, the dielectric layer is composed of the EDL with a thickness of d_1. When the electrode is functionalized with aptamer and blocking molecules, the dielectric layer thickness becomes d_1+d_2 where d_2 is the aptamer thickness (Fig. 1(b)). For this case, the

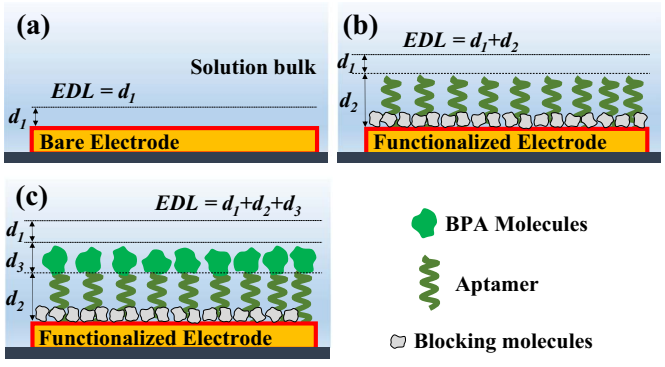

Fig. 1. Changes in EDL layer of the electrodes at different stages of sensor functionalization and BPA binding. (a) The electrode is clean and not functionalized, and the EDL thickness is d_1 . (b) The electrode is functionalized, and the EDL thickness becomes d_1 +d_2. (c) After binding reaction happens and BPA molecules bind to the aptamer, EDL thickness increase to d_1 +d_2 +d_3.

interfacial capacitance of the electrode before binding reaction is $C_{\text{int , before binding}} = A_{\text{int}}/((1/\varepsilon_b)d_2 + (1/\varepsilon_s)d_1)$, where A_{int} is the surface area of interfacial capacitance when the electrode is functionalized, ε_b and ε_s are the permittivities of the sample fluid and aptamer, respectively. When binding reaction happens, the dielectric thickness of the interfacial capacitance becomes the sum of d_1, d_2 and d_3 (Fig. 1(c)), and the interfacial capacitance becomes $C_{\text{int , after binding}} = A_{\text{int , b}}/((1/\varepsilon_b)(d_2 + d_3) + (1/\varepsilon_s)d_1)$, where d_3 is the thickness of BPA molecules and $A_{\text{int , b}}$ is the surface area of interfacial capacitance after binding. Based on the equations for $C_{\text{int , before binding}}$ and $C_{\text{int , after binding}}$ the binding of BPA molecules to the aptamer can be found by calculating the normalized capacitance change rate according to the following equation,

$$(C_{\text{int , after binding}} - C_{\text{int , before binding}})/C_{\text{int , before binding}} = -d_3/((d_2 + d_3) + (\varepsilon_b/\varepsilon_s)d_1)$$

. The calculated $\Delta C/C_{\text{int , before binding}}$ can be directly used as an indication of BPA molecules binding to the aptamer. Further, using normalized capacitance change rate instead of capacitance changes has the benefit of reducing inconsistences between sensors and will increase the repeatability of the method.

The sensor is composed of an interdigitated electrode (IDE) with 7 fingers. When the IDE is immersed in an electrolytic solution, neighboring fingers can be approximated by an equivalent electrical network as shown in Fig. 2(a), in which R_e is metallization resistance of the fingers, C_{int} is interfacial capacitance between the electrode and the electrolyte, R_{ct} is charge transfer resistance between the electrode and the electrolyte, R_s is electrolyte resistance, and C_s is electrolyte capacitance. Among these parameters, C_{int} is indicative of electrode surface conditions such as molecular deposition or nanostructure topologies. At low frequencies (lower than 100 kHz), C_{int} and R_s dominate the impedance network, and the equivalent electric network can be simplified as a series connection of two interfacial capacitances (C_{int}) and an electrolyte resistance R_s (Cui et al., 2013b) (Fig. 2(b)). Because two C_{int} are in series, the simplified circuit can be reduced to two elements of C_{eq} and R_s which $C_{eq} = C_{int}/2$, as shown in Fig. 2(b). When measuring the sensor impedance by an impedance analyzer, the measured impedance of the sensor is in the form of $Z_{sensor} = R - j/\omega C$, where, based on previous simplifications, R and C corresponds to R_s and $C_{eq} = C_{int}/2$, respectively (Fig. 2(b)). Therefore, any change in measured capacitance can be directly used to indicate the binding reaction of BPA molecules with aptamer.

2.1.2. AC electrokinetics for accelerated aptamer-BPA binding

In a conventional biosensor, the occurrence of binding reaction mostly depends on the diffusion of BPA molecules to the functionalized surfaces of sensor. For low abundant solution, accumulation of BPA molecules over specific sites may take hours or even days to reach a detectable range. An effective method for increasing the sensitivity and at the same time decreasing the response time is to generate directional microflows inside the solution to move target molecules toward functionalized sites. Based on our prior work (Cui et al., 2013b, 2015; Li et al., 2014; Rocha et al., 2016), by applying an inhomogeneous AC electric field to the sensor immersed in an aqueous solution, directional microflows toward electrode surface are induced inside the solution which greatly enriches target molecules at the sensor. All three major ACEK effects, dielectrophoresis (DEP), AC electroosmosis (ACEO) and AC electrothermal (ACET) effects, can be used to induce directional biomolecular movement (Lian et al., 2007b; Wu, 2008; Wu et al., 2005; Yuan et al., 2014). Our previous study on BPA detection revealed that for aquatic solutions with medium to high ionic strength (Cui et al., 2015), ACET effect is predominant in inducing directional microflows and long range convection of BPA molecules to the electrode surface, which is the mechanism used in this work for BPA enrichment.

ACET effect originates from uneven Joule heating of fluid, which generates thermal gradient∇T (Wu et al., 2007). The ∇T produces inhomogeneity in conductivities and permittivities as $\nabla\sigma = (\partial\sigma/\partial T)\nabla T$and $\nabla\varepsilon = (\partial\varepsilon/\partial T)\nabla T$. Consequently, $\nabla\varepsilon$ and $\nabla\sigma$ generate mobile electric charges ρ_E in the fluid bulk, by $\rho_E = \nabla.(\varepsilon E) = \nabla\varepsilon.\ E + \varepsilon\nabla.\ E$ and $(\partial\rho_E/\partial t) + \nabla.(\sigma E) = 0$ with $\partial/\partial t = i\omega$ in AC field, where ω is angular frequency. Through the induced charges, AC fields exert body forces on incompressible fluids as $F_E = \rho E$. Its time average is $\langle F_{ACET}\rangle = -0.5K_{et}(\omega).\nabla T.\ \varepsilon E_0^2$ where $K_{et}(\omega) = ((\partial\sigma/\partial T)/\sigma) - ((\partial\varepsilon/\partial T)/\varepsilon)(1/(1+\omega^2\tau_2))$ and $\tau = \varepsilon/\sigma$ is electrolyte charge relaxation time. In an aqueous system, $1/\varepsilon(\partial\varepsilon/\partial T) = -0.4\%/K$, $1/\sigma(\partial\sigma/\partial T) = -0.2\%/K$, so $k_{et}(\omega) = 0.022/K$ for AC frequency $\omega << 1/\tau$ leading to $\langle F_{ACET}\rangle = -0.011\cdot\nabla T\cdot\varepsilon E_0^2$. With planar electrodes, ACET effect will induce vortices above each electrode, and the microflows will convect the embedded particles towards the electrode surface (Lian et al., 2007a). Because ACET generates microflows independent of particle size, it is well suited for long range enrichment of nanoscale molecules such as BPA.

Fig. 3 schematically shows the operation mechanism of this sensor. ACET flow carries a mixture of bioparticles including BPA and interference particles such as Bisphenol S (BPS) and Bisphenol F (BPF) to the electrode's surface during capacitance measurement.

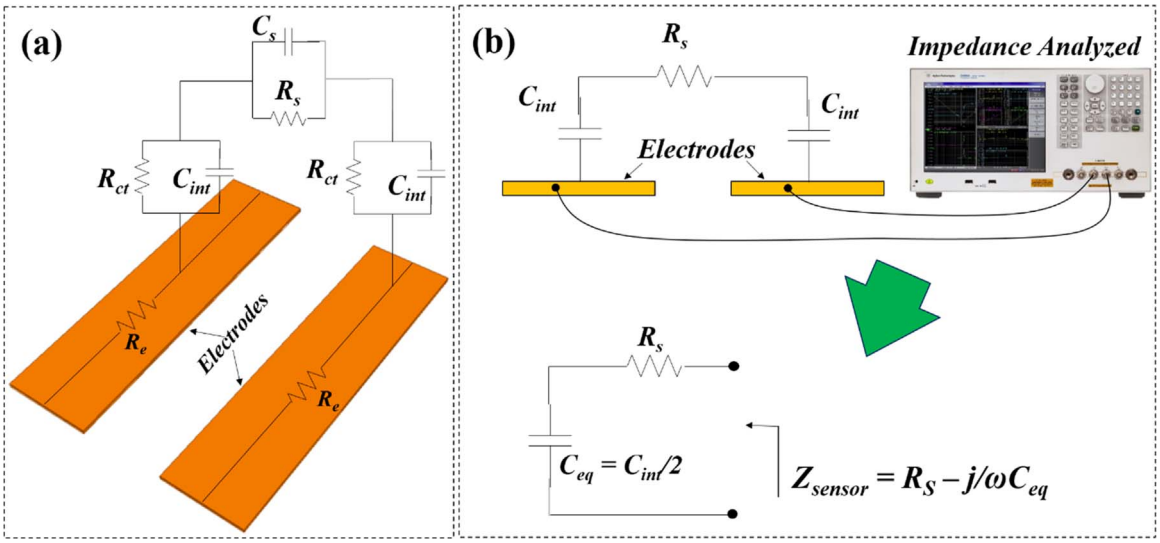

Fig. 2. (a) Equivalent circuit model of two nearby electrodes in an IDE sensor. (b) Simplified equivalent circuit model of the sensor at frequencies lower than 100 kHz.

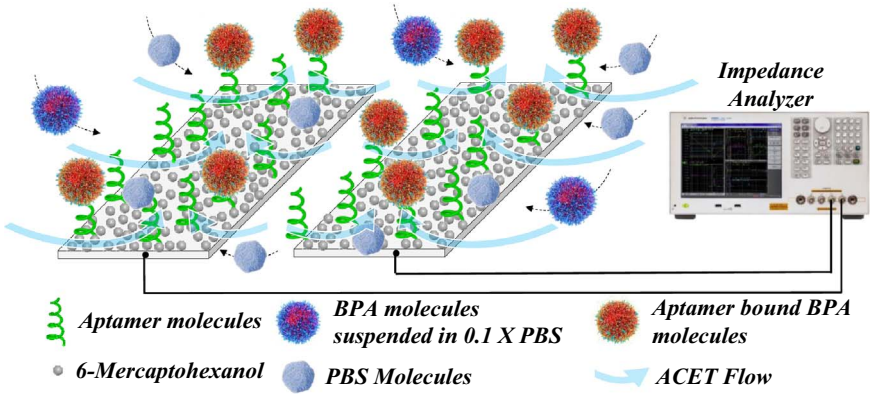

Fig. 3. Excitation of ACET effect is integrated into capacitance measurement during a BPA detection experiment. The ACET flows carry BPA particles toward functionalized sites and accelerate the sensor response.

Because the immobilized aptamer will bind only with BPA, binding of BPA increases the surface dielectric layer thickness and decreases the interfacial capacitance to achieve specific detection.

2.2. Experiments

2.2.1. Sensor fabrication

Pyralux 8525 R (DuPont, USA), a single-sided flexible copper cladded polyimide film, is used for the device prototyping and patterning by printed circuit board (PCB) technique. The copper layer thickness is 18 μm. The fabrication process is simple, rapid, low-cost, and can be performed by benchtop equipment. A detailed overview of the fabrication technique is provided in Fig. S1 of Supplementary Materials. The fabrication steps are as follows. 1) The layout of the device is drawn in Microsoft Visio software on a computer and then printed by a regular laser printer onto a piece of Toner Transfer Paper (PulsarProFX, CO, USA) (Fig. S1, a and b). 2) The Toner Transfer Paper is folded with a piece of PCB film in the middle. The Toner Transfer Paper covers both sides of the PCB film. The tri-layer is then rolled through a laminator (Apache, model AL13P) at a temperature of 188° C for around 30 s in order to transfer the pattern of Toner Transfer Paper onto the PCB film (Fig. S1, c). 3) A sheet of copper etch-resist film (Green TRF Foil, PulsarProFX) is then doubled and covers both sides of the PCB film. Again, the tri-layer is run though the laminator for 30 s (Fig. S1, d). 4) After the second lamination, the etch-resist film is peeled off from the PCB film. Only the previously patterned areas are covered by the etch-resist film (Fig. S1, d). 5) The PCB film is chemically etched in a ferric chloride solution (MG Chemicals) for approximately 10 min to yield the desired pattern (Fig. S1, e), then rinsed thoroughly by acetone, isopropyl alcohol and then running de-ionized (DI) water for 5 min in order to remove the etch-resist film from the electrode surface (Fig. S1, f). 6) Subsequently, gold electroplating is conducted in order to coat the sensor surface with a very thin layer of gold (Fig. S1, g). This process was done using an electroplating kit (Plug N′ Plate® Gold Electroplating Kit, Caswell, Inc., USA) for 5 min. Detailed description of electroplating process is provided in Supplementary Materials. 7) Finally, two lead wires are soldered to the electrode pads. The final fabricated device and a zoomed-in view of the electrode surface are shown in Fig. S2 in Supplementary Materials. Each electrode of the fabricated sensor has 500 μm width and 6.5 cm length, and the spacing between electrodes is 150 μm.

2.2.2. Food sample preparation

All chemical reagents including BPA aptamer were acquired from (Thermo Fisher Scientific, Waltham, MA). The sample solution used for ACEK capacitive assay was based on 0.1× PBS. The sequence of 5′ thiol modified BPA specific is 5′ -CCG GTG GGT GGTCAG GTG GGATAG CGT TCC GCG TAT GGC CCA GCG CAT CAC GGG TTC GCA CCA-3′. The blocking solution was 1.0 mM 6-mercaptohexanol dissolved in water, which was used for blocking the electrode surface after immobilizing aptamer. BPA (11.3 mg) was dissolved in 5 mL DMSO to make 10 mM BPA stock solution. Then, serial 1:10 dilutions with DMSO stock solution was conducted in order to make stock BPA concentrations of 1 μM, 100 nM, 10 nM, and 1 nM. After that, aforementioned BPA concentrations were further diluted 1:1,000,000 in 0.1× PBS to make the working solutions of 1 pM, 100 fM, 10 fM, and 1 fM for testing. The concentrations of DMSO were kept constant in all the working solutions. To test BPA levels in canned food, two different brands of food were purchased in November 2015 from a local retail store. Brand 1, a national brand, was French Style Green Beans in metal can, but no coating material information is available; and Brand 2 was Sweet Peas in Polypropylene (body and lid) container. None of the two Brands were labeled as BPA free. Only the liquid portion from the cans was used for BPA analysis.

2.2.3. Sensor preparation and functionalization

Before functionalization of electrode surface, the electrodes were thoroughly cleaned. The following cleaning procedure has been previously proven to clean the electrode surface effectively, which was confirmed by significant increase of the interfacial capacitance at the solution/electrode boundary (Cui et al., 2013a). The fabricated sensors were immersed into an acetone tank on a shaker for 15 min. Then, they were rinsed by isopropyl alcohol for 10 s and another 10 s with deionized water. After drying the electrodes surface by an air gun, they were plasma treated by putting the electrodes into a PE-50 Plasma Cleaner (Plasma Etch Inc., NV, USA) at the power of 45 W for 5 min. Then the electrode surface was ready to be functionalized.

Sensor functionalization includes immobilization of BPA-specific aptamer and blocking molecules over electrodes. To immobilize aptamer, 10 μL of BPA-specific aptamer (2 μM, diluted in purified water) was loaded over sensor. The sensor was incubated at room temperature in a humidor for 12 h. Then, its surface was blocked by 10 μL of 1.0 mM 6-mercaptohexanol for 3 h. After that, the sensor was ready for BPA binding assay.

2.2.4. Experimental method

The functionalized sensor was connected to a high precision impedance analyzer (Agilents 4294A), as in Fig. S3 in Supplementary Materials, and its capacitance was recorded through its LAN port onto a computer using software Data Transfer V3.0 (SEKONICs). ACET-based capacitive assay was done by applying an AC signal with specific frequency and amplitude directly to the sensor for 20 s to induce ACET effect, and simultaneously measuring its capacitance changes. Then, the slope of the normalized capacitance versus time (%/min) was calculated to indicate the binding level of BPA. To ensure that the

capacitance changes of the sensor was due to BPA binding with aptamer instead of artifacts, control tests were carried out as well. One was testing the blank buffer solution (0.1× PBS with DMSO) without BPA samples by a functionalized sensor, and the other one was testing BPA samples on the electrodes that were blocked without aptamer immobilization (dummy electrodes). The specificity of sensor was also investigated by testing BPF and BPS, the structural variants of bisphenol and the common BPA alternatives used by industries.

The frequency and amplitude of the test signal was chosen to be 500 Hz and 600 mV, respectively. 500 Hz was chosen as the test frequency because the impedance spectra of the sensor, when loaded with 0.1× PBS, was the most capacitive around 500 Hz and the measured impedance was mostly interfacial capacitance. Fig. S4 in Supplementary Materials shows the phase curves of the impedance spectra of three different sensors which were prepared and functionalized based on previously described assay method and loaded with 10 μL of 0.1× PBS. As apparent from Fig. S4, the phase angles were close to their minimum around 500 Hz. Hence, the measured impedance ($Z_{sensor} = R_S - j/\omega C_{eq}$ where $C_{eq} = C_{\text{int}}/2$) was more capacitive and the measured data became more accurate with minimum noise. As for the test signal's amplitude, by increasing the amplitude, the ACET flow became stronger and could collect more BPA molecules. The sensor response for control solution (without BPA) and 100 fM BPA at different applied voltages with a fixed frequency of 500 Hz is shown in Fig. S5 in Supplementary Materials. However, the amplitude cannot be increased arbitrarily, because higher voltages may lead to detachment of functionalized layer over electrode surface and lead to malfunction of the sensor.

3. Results and discussion

3.1. Sensor impedance

We first extracted and studied the equivalent circuit model of the sensor to ensure that the measured capacitive data were mostly from the interfacial capacitor changes (caused by the binding of BPA to aptamer). If the capacitive data were from other sources, the measurements would become unreliable. The impedance spectra of the sensor were measured over a frequency range of 40–110 MHz. By curve-fitting of the measured data using the impedance network shown in Fig. 2(a), the equivalent circuit parameters could be extracted. The measured data and curve-fitting result are shown in Fig. S4 of Supplementary Materials with good agreement between the measured and fitted data. The values of the circuit parameters were extracted as follow: R_e =8 Ω, C_{int} =47 nF, R_{ct} =23 kΩ, R_s =550 Ω and C_s =9.7 pF.

At low frequencies (lower than 100 kHz), the equivalent circuit model could be further simplified. For example, at 1 kHz, the reactance of C_{int} and C_s was calculated to be 3.387 kΩ ($<<R_{ct}$ =23 kΩ) and 16.416 MΩ ($>>R_s$ =550 Ω), respectively. Hence, the C_{int} and R_s dominated the impedance network and the equivalent electric network could be simplified as a series connection of two interfacial capacitances (C_{int}) and an electrolyte resistance R_s (Cui et al., 2013b) (Fig. 2(b)). Because two C_{int} were in series, the simplified circuit could be reduced to two elements of C_{eq} and R_s which $C_{eq} = C_{int}/2$, as shown in Fig. 2(b).

3.2. Dose response and limit of detection (LOD) extraction

Fig. 4(a) shows the normalized C_{int} changes over time for the functionalized sensor and dummy electrodes. As shown in Fig. 4(a), the normalized capacitance changes over time increased with higher BPA concentration. The slope was −4.446%/min for 1 fM BPA and reaches −7.38%/min, −10.674%/min, −12.67%/min, and −16.14%/min for 10 fM, 100 fM, 1 pM and 10 pM of BPA, respectively. The capacitance change rate for the blank control solution without BPA was −1.26%/min, which is very low in comparison to those triggered by BPA in the samples. Moreover, the results of the dummy test showed slope of 0.036%/min for 1 pM and 0.012%/min for 10 pM of BPA. These experiments supported that specific binding of BPA molecules with immobilized aptamer was indeed directly responsible for the changes of C_{int}..

To obtain the dose response and the limit of detection (LOD) of the sensor, BPA samples with concentration range from 1 fM to 10 pM were tested using functionalized sensors. Each BPA sample was injected into a chamber located over the sensor. The capacitance of the sensor was sampled 201 times during the test, then normalized capacitance change rate (-d|C|/dt, where |C| means normalized capacitance) was calculated for each BPA concentration. Each concentration was tested four times with a new functionalized sensor each time. The response of the sensor for control solution (0.1×PBS with DMSO), which was used to dilute BPA samples, was 0.6615 ± 0.608369%/min. The sensor response (-d|C|/dt) increased with BPA concentration from 1 fM to 10 pM, with 4.696 ± 0.618%/min for 1 fM, 7.58 ± 0.34%/min for 10 fM, 10.485 ± 1.035%/min for 100 fM, 13.036 ± 0.6179%/min for 1pM and 15.93 ± 0.816%/min for 10 pM BPA. The sensitivity of the sensor was extracted to be $-(d|C|/dt) = 1.2124 \ln(x) + 46.638$ where x was BPA concentration. The correlation coefficient R^2 for the linear fitting was 0.9995. As seen from Fig. 4(b), the sensor response has a wide linear range from 1 fM to 10 pM. The LOD of the sensor was defined as 3 standard deviations (± 0.608%/min) from the response of background solution (0.6615 ± 0.608369%/min) (Cui et al., 2016). Based on this definition, the cut-off value for sensor response (-d|C|/dt) was found to be 2.4866%/min. By substituting this value into the dose response equation, the LOD was calculated to be 152.93 aM.

3.3. Selectivity

The detection specificity of BPA sensor was investigated by testing two BPA analogs, Bisphenol S (BPS) and Bisphenol F (BPF). Both BPF and BPS may post similar health risk concerns as BPA and therefore could present as serious confounders interfere with our understanding of the impact of BPA exposure on human reproductive health (Sartain and Hunt, 2016). The specificity test was conducted in two sets of experiments. In the first set, 100 pM of BPS and BPF were tested separately on electrodes functionalized with BPA-specific aptamer following the same procedures as described in this paper. The second set of experiments conducted was to determine the specificity of the sensor to a low concentration of the BPA in the presence of BPA analogs. Solutions containing 1 pM BPA in the presence of 100 pM of BPS or 100 pM of BPF was prepared and tested. The results were summarized in Fig. 4(c). Each sample was tested four times on a new functionalized sensor each time.

As given in Fig. 4(c), the sensor responses (-d|C|/dt) for control solution, 100 pM BPF and 100 pM BPS were 0.6615 ± 0.6083%/min, 0.225 ± 0.1236%/min and 0.4122 ± 0.31757%/min, respectively. The sensor responses for 100 pM BPS and BPF were close to that of the control solution and all were below the cut-off value for the sensor. Hence, the sensor was considered unresponsive to BPS and BPF. Moreover, the sensor responses for 1 pM BPA in the presence of 100 pM BPF or BPS were 12.249 ± 1.0036%/min and 13.3455 ± 1.2672%/min, respectively, which were 94% and 102.37% of the sensor response to 1 pM BPA without any interference (13.0365 ± 0.6179%/min). These experiments validated that the sensor is unresponsive to BPA analogs molecules, and has the capability to detect BPA molecules in the presence of BPS and BPF.

3.4. Application of biosensor to real food samples

In order to study the performance and feasibility of this biosensor in a real life setting, the device was employed to determine trace amounts of BPA spiked in canned food samples, a complex matrix.

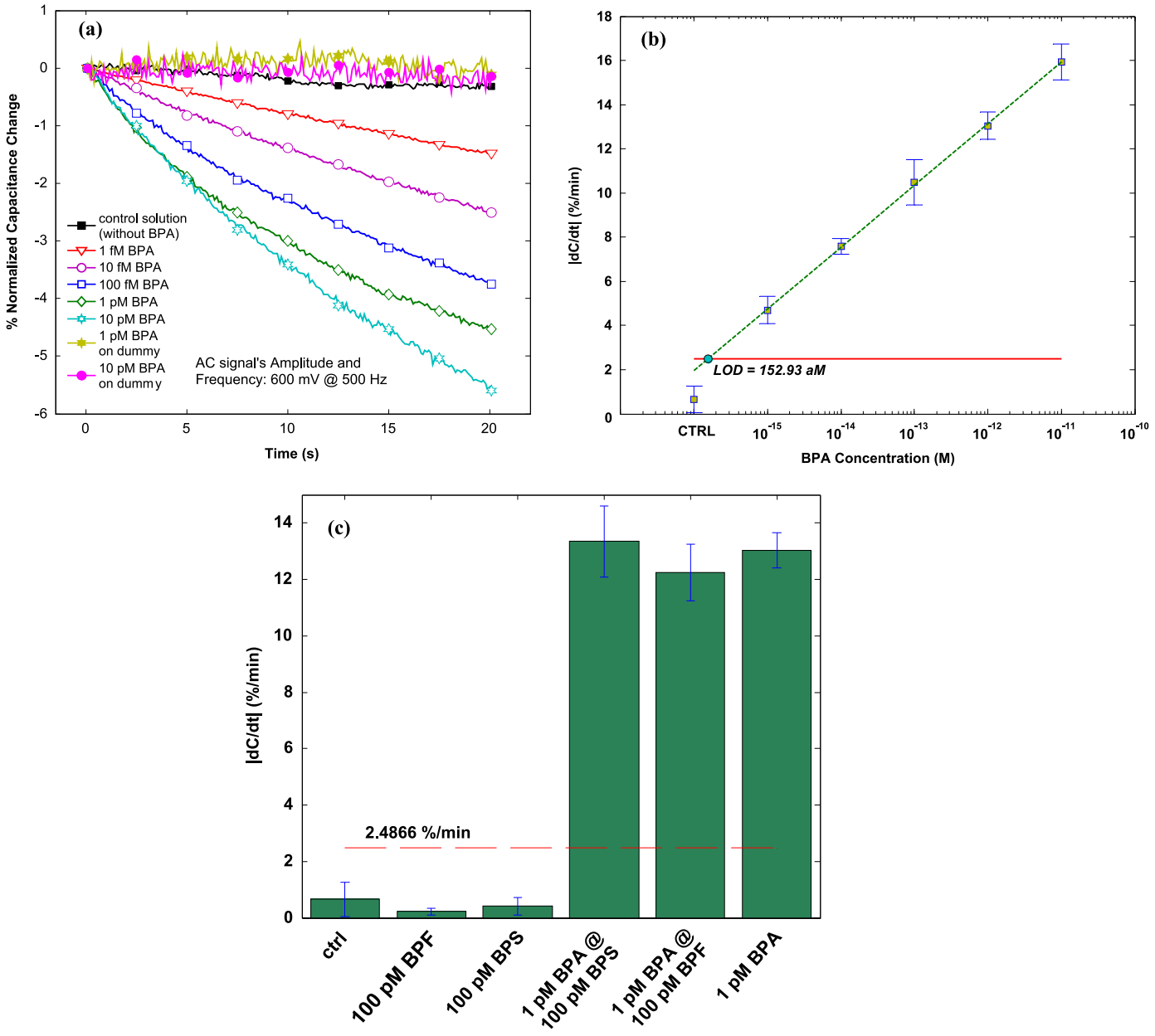

Fig. 4. (a) Normalized C_{int} changes with time for blank buffer, dummy electrodes and different concentrations of BPA. (b) Sensor response to different concentrations of BPA samples. . The dotted line is the extracted standard curve. Its slope represents the sensor sensitivity. The horizontal line indicates the LOD (152.93 aM) of the sensor. Error bars represent standard deviation. (c) Sensor specificity. The response of the sensor for the background, 100 pM BPF and 100 pM BPS are below the cut-off line. The sensor response for 1 pM BPA in the presence of 100 pM BPS and BPF is very close to the sensor response to 1 pM BPA. High resolution version of the figures are provided in Figs. S6–S8 of the Supplementary Materials.

Liquid portion of food samples from two different brands were collected and diluted in water. Two dilutions at 1:100 and 1:1000 were prepared for Brand 1 to determine the background level of BPA. For each dilution, the test was conducted on five different functionalized sensors. The mean value for -d|C|/dt was calculated to be 11.475 and 8.462. Substituting them into the dose response equation of the sensor (section 4.2), the detected background values of BPA were 253.85 fM for 1:100 dilution and 21.13 fM for 1:1000 dilution, corresponding to the concentrations of 25.385 and 21.13 pM in neat sample, respectively. The results derived from different dilutions (1:100 and 1:1000) were in close agreement, supporting the validity of this BPA sensor. Next, the food samples were spiked with known levels of BPA and recovery tests were conducted. The 1:1000 dilution of brand 1 was spiked with 10 and 50 fM of BPA. The measured mean values of -d|C|/dt for 10 and 50 fM spiking were calculated to be 8.953 and 9.962 which corresponded to 31.71 and 72.82 fM of BPA, respectively. At 1:100 dilution, 50 fM of BPA was spiked and the measured mean value of -d|C|/dt was 11.706 which equaled to 306.91 fM of BPA. To calculate% recovery of the spiked results, the following equation was used, $\% R = ((A - B)/S) \times 100$, in which A was sensor response after spiking, B was sensor response before spiking and S is spiked value. Based on this equation, the % recovery for 1:1000 dilution spiked with 10 and 50 fM BPA were 105.8% and 103.38%, respectively. For 1:100 dilution with 50 fM spiking, the recovery was 106.12%. For Brand 2, only 1:100 dilution was used for experiments due to low level background BPA in the sample. Prior to the spiking, the -d|C|/dt level was 7.638, which corresponded to 10.71 fM of BPA in diluted sample or 1.07 pM BPA in the initial sample solution. For recovery, 10 and 50 fM of BPA were spiked in 1:100 dilution of Brand 2 sample. The -d|C|/dt response of the sensor were 8.282 and 9.772 which corresponded to 18.22 and 62.28 fM of BPA for 10 and 50 fM BPA respectively. The calculated percentage of recovery rates were

Table 2
Analysis of canned food samples spiked with different BPA concentration.

		Detected (fM)	Added (fM)	Measured (fM)	Recovered (%)
Brand 1	1:100 dilution	253.85	50	306.91	106.12
	1:1000 dilution	21.13	10	31.71	105.8
			50	72.82	103.38
Brand 2 (1:100 dilution)		10.71	10	18.22	75.1
			50	62.28	103.14

75.1% and 103.14%, respectively. The real food sample experiments and recovery results are summarized in Table 2. The results extracted here are compatible with previous reports regarding BPA level in food samples (Cao et al., 2010; Goodson et al., 2002; Imanaka et al., 2001).

4. Conclusion

We reported a highly sensitive, rapid, low cost and simple to fabricate and operate aptasensor for detection of BPA. The presented BPA sensor was fabricated by benchtop equipment and low-cost materials through PCB technique. AC-electrothermal effect was used for transport of BPA molecules towards electrode in order to accelerate the binding process and to decrease the response time of the sensor to as low as 20 s. The sensor showed a wide linear detecting range for BPA from 1 fM to 10 pM with a limit of detection of 152.93 aM, which was lower than others reported in the literature. Moreover, it presented very good reproducibility and selectivity. The successful application of this sensor in canned food samples demonstrated its utility for on-site trace analyzes of BPA.

Acknowledgements

H. Mirzajani and C. Cheng gratefully acknowledge the financial support from The University of Tennessee (UT) Center for Wildlife Health. H. Mirzajani also thanks the financial support from the Ministry of Science, Research and Technology (MSRT) of Iran. J. Wu and J. Chen acknowledge the support of UT Initiative for Point Detection and Nanobiosensing.

Appendix A. Supplementary material

Supplementary data associated with this article can be found in the online version at http://dx.doi.org/10.1016/j.bios.2016.09.109.

References

Authority, E., 2015. Scientific opinion on the risks to public health related to the presence of bisphenol A (BPA) in foodstuffs. EFSA J. 13, 1.
Brogden, K.A., 2005. Antimicrobial peptides: pore formers or metabolic inhibitors in bacteria? Nat. Rev. Microbiol. 3 (3), 238–250.
Cao, X.-L., Corriveau, J., Popovic, S., 2010. Bisphenol A in canned food products from Canadian markets. J. Food Protection® 73 (6), 1085–1089.
Chen, J., Zhou, S., 2016. Label-free DNA Y junction for bisphenol A monitoring using exonuclease III-based signal protection strategy. Biosens. Bioelectron. 77, 277–283.
Cheng, C., Wang, S., Wu, J., Yu, Y., Li, R., Eda, S., Chen, J., Feng, G., Lawrie, B.J., Hu, A., 2016. Bisphenol-A sensors on polyimide fabricated by laser direct writing for on-site river water monitoring at attomolar concentration. ACS Appl. Mater. Interfaces.
Chung, E., Jeon, J., Yu, J., Lee, C., Choo, J., 2015. Surface-enhanced Raman scattering aptasensor for ultrasensitive trace analysis of bisphenol A. Biosens. Bioelectron. 64, 560–565.
Crain, D.A., Eriksen, M., Iguchi, T., Jobling, S., Laufer, H., LeBlanc, G.A., Guillette, L.J., 2007. An ecological assessment of bisphenol-A: evidence from comparative biology. Reprod. Toxicol. 24 (2), 225–239.
Cui, H., Cheng, C., Wu, J., Eda, S., 2013a. Rapid detection of progesterone by commercially available microelectrode chips. IEEE Sensors, 1–4, (IEEE).
Cui, H., Li, S., Yuan, Q., Wadhwa, A., Eda, S., Chambers, M., Ashford, R., Jiang, H., Wu, J., 2013b. An AC electrokinetic impedance immunosensor for rapid detection of tuberculosis. Analyst 138 (23), 7188–7196.
Cui, H., Wu, J., Eda, S., Chen, J., Chen, W., Zheng, L., 2015. Rapid capacitive detection of femtomolar levels of bisphenol A using an aptamer-modified disposable microelectrode array. Microchim. Acta 182 (13–14), 2361–2367.
Cui, H., Cheng, C., Lin, X., Wu, J., Chen, J., Eda, S., Yuan, Q., 2016. Rapid and sensitive detection of small biomolecule by capacitive sensing and low field AC electrothermal effect. Sens. Actuators B: Chem. 226, 245–253.
FDA, 2014. Bisphenol A (BPA): Use in Food Contact Application. U.S. Food and Drug Administration (FDA).
Feng, J., Xu, L., Cui, G., Wu, X., Ma, W., Kuang, H., Xu, C., 2016. Building SERS-active heteroassemblies for ultrasensitive Bisphenol A detection. Biosens. Bioelectron. 81, 138–142.
Gao, Y., Cao, Y., Yang, D., Luo, X., Tang, Y., Li, H., 2012. Sensitivity and selectivity determination of bisphenol A using SWCNT–CD conjugate modified glassy carbon electrode. J. Hazard. Mater. 199, 111–118.
Goodson, A., Summerfield, W., Cooper, I., 2002. Survey of bisphenol A and bisphenol F in canned foods. Food Addit. Contam. 19 (8), 796–802.
Guo, X., Wu, S., Duan, N., Wang, Z., 2016. Mn2+-doped NaYF4: yb/er upconversion nanoparticle-based electrochemiluminescent aptasensor for bisphenol A. Anal. Bioanal. Chem., 1–9.
Hoyos-Nogués, M., Brosel-Oliu, S., Abramova, N., Muñoz, F.-X., Bratov, A., Mas-Moruno, C., Gil, F.-J., 2016. Impedimetric antimicrobial peptide-based sensor for the early detection of periodontopathogenic bacteria. Biosens. Bioelectron. 86, 377–385.
Huo, X., Chen, D., He, Y., Zhu, W., Zhou, W., Zhang, J., 2015. Bisphenol-A and Female Infertility: a Possible Role of Gene-Environment Interactions. Int. J. Environ. Res. Public Health 12 (9), 11101–11116.
Imanaka, M., Sasaki, K., Nemoto, S., Ueda, E., Murakami, E., Miyata, D., Tonogai, Y., 2001. Determination of bisphenol A in foods using GC/MS. Shokuhin eiseigaku zasshi. J. Food Hyg. Soc. Jpn. 42 (2), 71–78.
Kim, K.S., Jang, J.-r, Choe, W.-S., Yoo, P.J., 2015. Electrochemical detection of Bisphenol A with high sensitivity and selectivity using recombinant protein-immobilized graphene electrodes. Biosens. Bioelectron. 71, 214–221.
Kim, S.G., Lee, J.S., Jun, J., Shin, D.H., Jang, J., 2016. Ultrasensitive Bisphenol A Field-Effect Transistor Sensor Using an Aptamer-Modified Multichannel. Carbon Nanofiber Transducer ACS Appl. Mater. Interfaces 8 (10), 6602–6610.
Kochana, J., Wapiennik, K., Kozak, J., Knihnicki, P., Pollap, A., Woźniakiewicz, M., Nowak, J., Kościelniak, P., 2015. Tyrosinase-based biosensor for determination of bisphenol A in a flow-batch system. Talanta 144, 163–170.
Li, H., Wang, W., Lv, Q., Xi, G., Bai, H., Zhang, Q., 2016a. Disposable paper-based electrochemical sensor based on stacked gold nanoparticles supported carbon nanotubes for the determination of bisphenol A. Electrochem. Commun. 68, 104–107.
Li, S., Cui, H., Yuan, Q., Wu, J., Wadhwa, A., Eda, S., Jiang, H., 2014. AC electrokinetics-enhanced capacitive immunosensor for point-of-care serodiagnosis of infectious diseases. Biosens. Bioelectron. 51, 437–443.
Li, Y., Zhai, X., Liu, X., Wang, L., Liu, H., Wang, H., 2016b. Electrochemical determination of bisphenol A at ordered mesoporous carbon modified nano-carbon ionic liquid paste electrode. Talanta 148, 362–369.
Lian, M., Islam, N., Wu, J., 2007a. AC electrothermal manipulation of conductive fluids and particles for lab-chip applications. Nanobiotechnol. IET 1 (3), 36–43.
Lian, M., Islam, N., Wu, J., 2007b. AC electrothermal manipulation of conductive fluids and particles for lab-chip applications. IET Nanobiotechnol. 1 (3), 36–43.
Mirzajani, H., Cheng, C., Wu, J., Ivanoff, C.S., Aghdam, E.N., Ghavifekr, H.B., 2016. Design and characterization of a passive, disposable wireless AC-electroosmotic lab-on-a-film for particle and fluid manipulation. Sens. Actuators B: Chem..
Moghadam, Z.A., Mirlohi, M., Pourzamani, H., Malekpour, A., 2012. Bisphenol A in "BPA free" baby feeding bottles. J. Res. Med. Sci.: Off. J. Isfahan Univ. Med. Sci. 17 (11), 1089.
Mustieles, V., Pérez-Lobato, R., Olea, N., Fernández, M.F., 2015. Bisphenol A: human exposure and neurobehavior. NeuroToxicology 49, 174–184.
Oppeneer, S.J., Robien, K., 2015. Bisphenol A exposure and associations with obesity among adults: a critical review. Public Health Nutr. 18 (10), 1847–1863.
Pan, D., Gu, Y., Lan, H., Sun, Y., Gao, H., 2015. Functional graphene-gold nano-composite fabricated electrochemical biosensor for direct and rapid detection of bisphenol A. Anal. Chim. Acta 853, 297–302.
Paseiro-Cerrato, R., Noonan, G.O., Begley, T.H., 2016. Evaluation of long term migration testing from cans coatings into food simulants: polyester coatings. J. Agric. Food Chem..
Reza, K.K., Ali, M.A., Srivastava, S., Agrawal, V.V., Biradar, A., 2015. Tyrosinase conjugated reduced graphene oxide based biointerface for bisphenol A sensor. Biosens. Bioelectron. 74, 644–651.
Rocha, A.M., Yuan, Q., Close, D.M., O'Dell, K.B., Fortney, J.L., Wu, J., Hazen, T.C., 2016. Rapid detection of microbial cell abundance in aquatic systems. Biosens. Bioelectron..

Sartain, C.V., Hunt, P.A., 2016. An old culprit but a new story: bisphenol A and "NextGen" bisphenols. Fertil. Steril..
Shao, B., Han, H., Hu, J., Zhao, J., Wu, G., Xue, Y., Ma, Y., Zhang, S., 2005. Determination of alkylphenol and bisphenol A in beverages using liquid chromatography/electrospray ionization tandem mass spectrometry. Anal. Chim. Acta 530 (2), 245–252.
Singh, N., Reza, K.K., Ali, M.A., Agrawal, V.V., Biradar, A., 2015. Self assembled DC sputtered nanostructured rutile TiO 2 platform for bisphenol A detection. Biosens. Bioelectron. 68, 633–641.
Song, S., Wang, L., Li, J., Fan, C., Zhao, J., 2008. Aptamer-based biosensors. TrAC Trends Anal. Chem. 27 (2), 108–117.
Tominaga, T., Negishi, T., Hirooka, H., Miyachi, A., Inoue, A., Hayasaka, I., Yoshikawa, Y., 2006. Toxicokinetics of bisphenol A in rats, monkeys and chimpanzees by the LC–MS/MS method. Toxicology 226 (2), 208–217.
Wang, J.-Y., Su, Y.-L., Wu, B.-H., Cheng, S.-H., 2016. Reusable electrochemical sensor for bisphenol A based on ionic liquid functionalized conducting polymer platform. Talanta 147, 103–110.
Wang, X., Reisberg, S., Serradji, N., Anquetin, G., Pham, M.-C., Wu, W., Dong, C.-Z., Piro, B., 2014. E-assay concept: detection of bisphenol A with a label-free electrochemical competitive immunoassay. Biosens. Bioelectron. 53, 214–219.
Wang, X., Lu, X., Wu, L., Chen, J., 2015. 3D metal-organic framework as highly efficient biosensing platform for ultrasensitive and rapid detection of bisphenol A. Biosens. Bioelectron. 65, 295–301.
Wu, J., 2008. Interactions of electrical fields with fluids: laboratory-on-a-chip applications. IET Nanobiotechnol. 2 (1), 14–27.
Wu, J., Ben, Y., Chang, H.-C., 2005. Particle detection by electrical impedance spectroscopy with asymmetric-polarization AC electroosmotic trapping. Microfluid. Nanofluidics 1 (2), 161–167.
Wu, J., Lian, M., Yang, K., 2007. Micropumping of biofluids by alternating current electrothermal effects. Appl. Phys. Lett. 90 (23), (234103-234103).
Wu, L., Deng, D., Jin, J., Lu, X., Chen, J., 2012. Nanographene-based tyrosinase biosensor for rapid detection of bisphenol A. Biosens. Bioelectron. 35 (1), 193–199.
Xue, F., Wu, J., Chu, H., Mei, Z., Ye, Y., Liu, J., Zhang, R., Peng, C., Zheng, L., Chen, W., 2013. Electrochemical aptasensor for the determination of bisphenol A in drinking water. Microchim. Acta 180 (1–2), 109–115.
Yang, L., Zhao, H., Fan, S., Li, B., Li, C.-P., 2014. A highly sensitive electrochemical sensor for simultaneous determination of hydroquinone and bisphenol A based on the ultrafine Pd nanoparticle@ TiO 2 functionalized SiC. Anal. Chim. Acta 852, 28–36.
Yoon, Y., Westerhoff, P., Snyder, S.A., Esparza, M., 2003. HPLC-fluorescence detection and adsorption of bisphenol A, 17β-estradiol, and 17α-ethynyl estradiol on powdered activated carbon. Water Res. 37 (14), 3530–3537.
Yoshida, H., Harada, H., Nohta, H., Yamaguchi, M., 2003. Liquid chromatographic determination of bisphenols based on intramolecular excimer-forming fluorescence derivatization. Anal. Chim. Acta 488 (2), 211–221.
Yu, P., Liu, Y., Zhang, X., Zhou, J., Xiong, E., Li, X., Chen, J., 2016. A novel electrochemical aptasensor for bisphenol A assay based on triple-signaling strategy. Biosens. Bioelectron. 79, 22–28.
Yuan, Q., Yang, K., Wu, J., 2014. Optimization of planar interdigitated microelectrode array for biofluid transport by AC electrothermal effect. Microfluid. Nanofluidics 16 (1–2), 167–178.
Zehani, N., Fortgang, P., Lachgar, M.S., Baraket, A., Arab, M., Dzyadevych, S.V., Kherrat, R., Jaffrezic-Renault, N., 2015. Highly sensitive electrochemical biosensor for bisphenol A detection based on a diazonium-functionalized boron-doped diamond electrode modified with a multi-walled carbon nanotube-tyrosinase hybrid film. Biosens. Bioelectron. 74, 830–835.
Zhou, L., Wang, J., Li, D., Li, Y., 2014. An electrochemical aptasensor based on gold nanoparticles dotted graphene modified glassy carbon electrode for label-free detection of bisphenol A in milk samples. Food Chem. 162, 34–40.
Zhu, L., Cao, Y., Cao, G., 2014. Electrochemical sensor based on magnetic molecularly imprinted nanoparticles at surfactant modified magnetic electrode for determination of bisphenol A. Biosens. Bioelectron. 54, 258–261.
Zhu, Y., Cai, Y., Xu, L., Zheng, L., Wang, L., Qi, B., Xu, C., 2015a. Building an aptamer/graphene oxide FRET biosensor for one-step detection of bisphenol A. ACS Appl. Mater. Interfaces 7 (14), 7492–7496.
Zhu, Y., Zhou, C., Yan, X., Yan, Y., Wang, Q., 2015b. Aptamer-functionalized nanoporous gold film for high-performance direct electrochemical detection of bisphenol A in human serum. Anal. Chim. Acta 883, 81–89.